Meiotic arrest and aneuploidy in MLH3-deficient mice

Steven M. Lipkin[1,2], Peter B. Moens[3], Victoria Wang[2], Michelle Lenzi[4], Dakshine Shanmugarajah[2,5], Abigail Gilgeous[4], James Thomas[5], Jun Cheng[6], Jeffrey W. Touchman[5], Eric D. Green[5], Pam Schwartzberg[6], Francis S. Collins[2,5] & Paula E. Cohen[4]

Published online: 1 July 2002, doi:10.1038/ng931

MutL homolog 3 (Mlh3) is a member of a family of proteins conserved during evolution and having dual roles in DNA mismatch repair and meiosis[1,2]. The pathway in eukaryotes consists of the DNA-binding components, which are the homologs of the bacterial MutS protein (MSH 2–6), and the MutL homologs, which bind to the MutS homologs and are essential for the repair process. Three of the six homologs of MutS that function in these processes, Msh2, Msh3 and Msh6, are involved in the mismatch repair of mutations, frameshifts and replication errors[2,3], and two others, Msh4 and Msh5, have specific roles in meiosis[4–10]. Of the four MutL homologs, Mlh1, Mlh3, Pms1 and Pms2, three are involved in mismatch repair and at least two, Pms2 and Mlh1, are essential for meiotic progression in both yeast and mice[2,3,11–14]. To assess the role of Mlh3 in mammalian meiosis, we have generated and characterized *Mlh3*$^{-/-}$ mice[15]. Here we show that *Mlh3*$^{-/-}$ mice are viable but sterile. Mlh3 is required for Mlh1 binding to meiotic chromosomes and localizes to meiotic chromosomes from the mid pachynema stage of prophase I. *Mlh3*$^{-/-}$ spermatocytes reach metaphase before succumbing to apoptosis, but oocytes fail to complete meiosis I after fertilization. Our results show that Mlh3 has an essential and distinct role in mammalian meiosis.

We examined Mlh3 localization on meiotic chromosomes (Fig. 1) in mouse spermatocytes by immunolocalization studies with antisera against Mlh3. Mlh3 foci appeared in early pachynema of prophase I (Fig. 1*a*), peaked by late pachynema and persisted until early diplonema (Fig. 1). Mlh3 foci associated exclusively with paired regions of chromosome cores in diplotene spermatocytes (Fig. 1), which is consistent with the localization of Mlh3 to true chiasmata after desynapsis.

Similar to the distribution of Mlh1 (refs 12,16,17), about 1–2 Mlh3 foci were observed on wildtype chromosomes at mid to late pachynema. Double-labeling experiments for Mlh3 and Mlh1 showed tight spatial and temporal colocalization on chro-

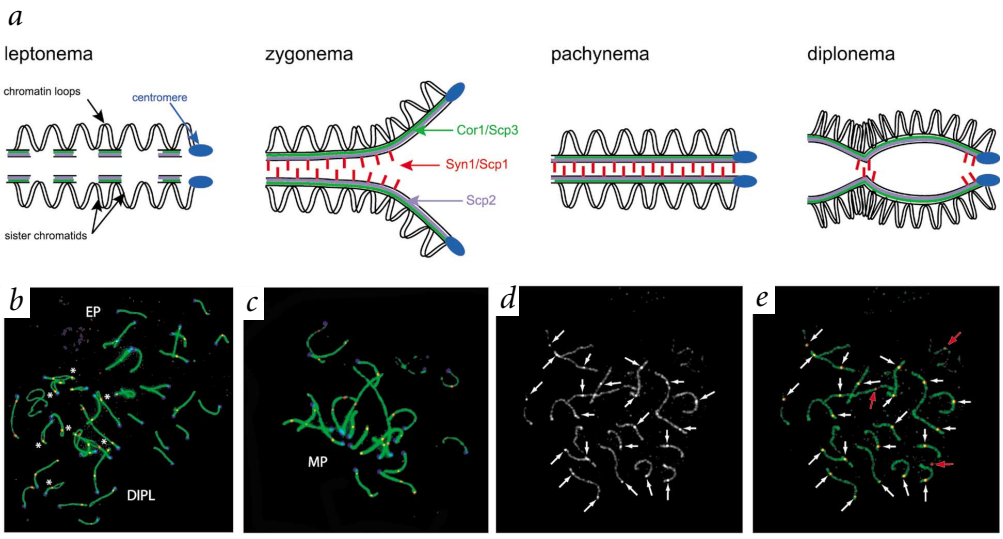

Fig. 1 Localization of Mlh3 to male mouse chromosomes at pachynema and diplonema stages of meiosis I. ***a***, The four stages of prophase I. In leptonema, sister chromatids acquire short chromosome core segments and begin the homology searching and recognition process. Electron-dense protein foci or early recombination nodules appear along each homolog and are thought to promote interactions between homologs, as well as to be the sites of initiation of recombination in yeast. In zygonema, homologous chromosomes begin to synapse. Paired homologs then 'zipper' together during synapsis and are held in this state by the synaptonemal complex, which comprises two axial elements containing Cor1 and a central element containing Syn1. In pachynema, homologous chromosomes become fully synapsed and remain so until diplonema, when the synaptonemal complex begins to break down and chromosomes move apart, remaining associated at their chiasmata. These crossover sites, which in yeast reflect the number of recombination nodules observed at zygonema, but in mammals are roughly one tenth as numerous, hold the homologs together until all chromosomes are aligned in metaphase I. ***b***,***c***, Mlh3 foci first appear in early pachynema (EP), peak in number by mid pachynema (MP) and persist until early diplonema (DIPL) in spermatocyte spreads from wildtype males. Foci at diplonema clearly show specific localization at regions of the chromosomes that maintain homologous synapsis, indicating specific localization at chiasma sites (asterisks in *b*). Mlh3 foci, in red (TRITC), are visualized on the green chromosome cores (FITC); centromeres are labeled in blue. ***d***,***e***, Colocalization of Mlh1 and Mlh3 on chromosomal cores from wildtype pachytene spermatocytes. Shown are synaptonemal complexes (green, FITC) with Mlh1 (bright green) and Mlh3 foci (TRITC, red). Mlh1 and Mlh3 localize to similar sites (white arrows indicate sites of colocalization) and at similar frequency on chromosomes from pachytene spermatocytes. Mlh3 foci are often observed without Mlh1 colocalized (red arrows in *e*), but never vice versa.

[1]Division of Hematology-Oncology, Department of Medicine, University of California, Irvine, California 92697, USA. [2]Genetics and Molecular Biology Branch, National Human Genome Research Institute, Bethesda, Maryland, USA. [3]Department of Biology, University of York, Toronto, Ontario M3J 1P3, Canada. [4]Department of Molecular Genetics, Albert Einstein College of Medicine, 1300 Morris Park Avenue, Bronx, New York, USA. [5]Genome Technology Branch and [6]Transgenic and Knock-out Core Facility, National Human Genome Research Institute, Bethesda, Maryland, USA. Correspondence should be addressed to S.M.L. (e-mail: slipkin@uci.edu) or P.E.C. (e-mail: pcohen@aecom.yu.edu).

mosomes at mid to late pachytene. Mlh3 foci occurred consistently without Mlh1 in early to mid pachynema (Fig. 1*c*), which suggests that Mlh3 either localizes before Mlh1 or can homodimerize in early pachynema. By contrast, we did not observe Mlh1 foci without Mlh3 in wildtype mice, but identified Mlh1–Mlh3 foci repeatedly in the XY bivalent pseudoautosomal region and obligate crossover site, which is consistent with their localization to sites of recombination.

To identify evolutionarily conserved elements in the *Mlh3* genomic locus, we sequenced the mouse *Mlh3* locus and compared it against the human gene *MLH3* (Web Fig. A online). Analysis showed that there is high similarity between exons 2 and 4–13 of human *MLH3* and mouse *Mlh3*. An alternatively spliced exon 3 is found in *Mlh3* that is not present in *MLH3*. Five blocks of homology, constituting less than 1% of the *MLH3* genomic locus, exist between *Mlh3* exons 1 and 2 (89% identity), 2 and 3 (76%), 3 and 4 (81%), 8 and 9 (88%), and in the 3′ region of exon 13 (85%). None of these five blocks of *Mlh3–MLH3* homology is predicted to encode exons.

To examine the meiotic role of Mlh3, we generated an *Mlh3*-null mouse allele (Fig. 2). The genotypes of F2 mice were consistent with expected mendelian ratios, which suggests that *Mlh3* is not essential for embryonic development. Northern and immunofluorescence analysis confirmed the generation of *Mlh3*-null mice (Fig. 2*b*,*c*).

As Mlh3 is proposed to participate in the repair of insertion–deletion errors at microsatellite repeat sequences[15,18], we tested nine markers (mononucleotide, dinucleotide and tetranucleotide) in $Mlh3^{-/-}$ fibroblasts. Microsatellite instability was detectable in fewer than 1% of these markers and was indistinguishable from that of wildtype fibroblasts (data not shown), which shows that Mlh3 is not required for mismatch repair.

The $Mlh3^{-/-}$ mice were healthy and showed no susceptibility to morbid cancer in the first 9 months of life (data not shown). Male and female $Mlh3^{-/-}$ mice mated normally but were infertile. The testes of $Mlh3^{-/-}$ mice were smaller than those of wildtype mice and showed azoospermia (Fig. 3). $Mlh3^{-/-}$ male testes showed severe depletion of spermatocytes but not of spermatogonia (Fig. 3*b*). Some spermatocytes were lost at pachynema, but most cells progressed to diplonema and metaphase (Fig. 3*c*,*e*). By metaphase, these cells showed missegregating chromosomes (Fig. 3*c*,*f*) and aneuploidy, which led to apoptosis (Fig. 3*g*–*i*). To verify that this infertility was due to absence of *Mlh3*, we complemented the *Mlh3*-null genotype with a human BAC transgene encoding *MLH3* to create transgenic mice bearing the human *MLH3* gene ($Mlh3^{-/-}Tg^{+}$; Fig. 3*j*). This transgene rescued fertility in both genders and restored spermatogenesis in males (Fig. 3*k*).

Proteins of the synaptonemal complex and Rad51 foci accumulated normally on prophase I chromosomes in the spermatocytes of $Mlh3^{-/-}$ mice, which suggests that early meiotic progression and chromosomal synapsis are unperturbed by the mutation (Fig. 4*a*–*c*). At pachynema, all autosomal bivalent chromosomes were fully synapsed (Fig. 4*b*), along with the pseudoautosomal region of the XY bivalent chromosome (Fig. 4*b*, arrow). Replication protein A (Rpa) localized to meiotic chromosomes from zygonema until mid pachynema in both wildtype and $Mlh3^{-/-}$ spermatocytes (data not shown). In wildtype spermatocytes, Rpa foci appeared and were gradually replaced with Mlh3-positive foci from mid pachynema (Fig. 4*d*). A few double-stained foci were evident (Fig. 4*d*), consistent with the transient colocalization of these two proteins, but Mlh3 persisted after all of the Rpa foci had disappeared (Figs 1*a* and 4*d*). We did not observe Rpa–Mlh1 foci, however, which suggests that there is a defined temporal order of binding to meiotic chromosomes: that is, Rpa binds first,

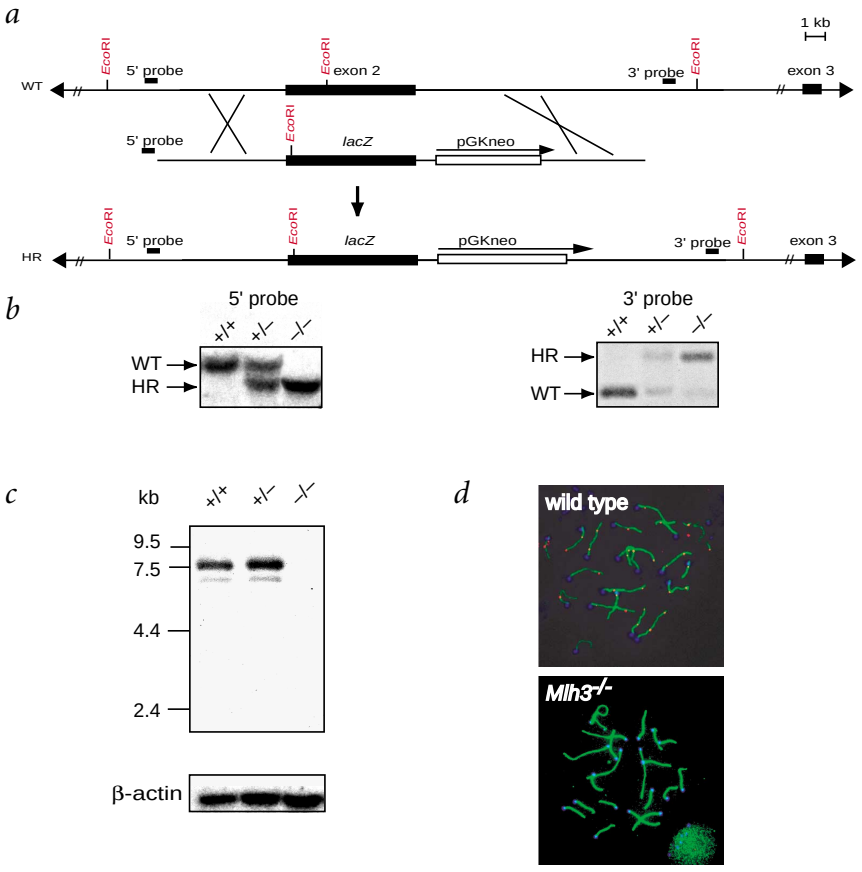

Fig 2. Generation of *Mlh3*-null mice. ***a***, Gene-targeting strategy. The *Mlh3* locus (WT), the homologous recombination targeting construct (HR vector) and the recombinant locus (HR) are shown. The HR 5′ flanking sequence (5′ flanking plus exon 1), exon 2 and the HR 3′ flanking sequence from intron 2 are boxed, as is the HR vector. The neomycin resistance cassette, *lacZ* gene and *Eco*RI sites are indicated. The diagnostic *Eco*RI digestion products for the wildtype and HR *Mlh3* locus that were probed are shown. Black boxes represent the 5′ and 3′ targeting-vector flanking probes. ***b***, Southern-blot hybridization. Tail DNA was digested with *Eco*RI and hybridized with 5′ or 3′ flanking probes. For 5′ HR, bands of 7.2 and 6.3 kb, corresponding to wildtype and targeted alleles, respectively, are observed. For 3′ HR, bands of 9.0 and 10.3 kb, corresponding to wildtype and targeted alleles, respectively, are observed. The residual hybridization at 9.0 kb in $Mlh3^{-/-}$ mice is due to contamination from wildtype mouse embryonic fibroblast feeder-layer cells, on which the embryonic stem cells are grown in culture. ***c***, Northern analysis. Testis mRNA (1 μg) from wildtype, $Mlh3^{+/-}$ and $Mlh3^{-/-}$ mice was hybridized with a probe comprising the complete *Mlh3* cDNA. A probe specific for human β-actin was subsequently hybridized to the same blot used as a control for mRNA quantity and quality. ***d***, Chromosomal immunolocalization of Mlh3 in wildtype and $Mlh3^{-/-}$ males. Mlh3 is localized with polyclonal rabbit serum against Mlh3 (red/yellow) on chromosomes during the meiosis I pachytene stage. Arrowheads indicate some of the Mlh3 wildtype chromosomal foci. Chromosomes are labeled with an antibody against Cor1 (green); centromeres are visualized with antiserum against CREST (blue).

followed by Mlh3 and then Mlh1. Notably, although Mlh1 is localized in discrete foci during late pachynema in *Mlh*$^{+/+}$ spermatocytes (Fig. 4*e*), the absence of Mlh3 results in a failure to load Mlh1 onto chromosome cores at this, or any other, stage (Fig. 4*f*).

Wildtype homologous chromosomes began to repel one another in diplonema, but remained associated at sites of chiasmata. In *Mlh3*$^{-/-}$ spermatocytes, chromosomes separated abnormally (Fig. 4*g*), producing mostly univalent and a few bivalent chromosomes (Fig. 4*h*, arrows). Similar findings have been described for *Mlh1*$^{-/-}$ mice[12], although few or no persistent bivalent chromosomes were reported. In wildtype spermatocytes, recombination nodules were visible as 1–2 dense foci per chromosome located between the axial elements of the synaptonemal complex and directly on the central elements (Fig. 5*a*,*b*). Unexpectedly, no recombination nodules were observed on *Mlh3*$^{-/-}$ bivalent chromosomes at pachynema (Fig. 5*c*,*d*). Thus, although chromosomes remained synapsed until diplonema, presumably held together by remnants of the synaptonemal complex central element, the recombination nodules were either never formed or lost at pachynema.

Localization of Mlh3 on the pachytene chromosomes of wildtype oocytes was similar to that on male chromosomes (Fig. 6*a*). The *Mlh3*$^{-/-}$ female mice mated normally but were infertile. The ovaries of these mice were histologically normal (Fig. 6*b*,*c*), and follicles were observed at all developmental stages but did not produce viable oocytes, as assessed by *in vitro* fertilization. Similar to *Mlh1*$^{-/-}$ oocytes, *Mlh3*$^{-/-}$ oocytes showed abnormalities in extrusion of the first and second polar bodies after fertilization *in vitro* with wildtype spermatozoa (Table 1). But although more than 50% of wildtype fertilized oocytes successfully completed meiosis I and progressed to the two-cell stage, only 7% of *Mlh3*$^{-/-}$ oocytes progressed to the two-cell stage.

In summary, the chromosomal localization of Mlh1 and Mlh3 is restricted to pachynema, and their absence causes germ-cell apoptosis at diplonema. Of the two remaining MutL homologs, only Pms2, and not Pms1, has been implicated in mammalian meiosis. Spermatocyte defects in *Pms2*$^{-/-}$ mice (axial element fragmentation and nonhomologous chromosome synapsis) are first seen in zygonema[13], which suggests that Pms2 is required before Mlh1 and Mlh3 in males but is not required in females. The role of Pms1 in meiosis is not clear, as *Pms1*$^{-/-}$ mice are reported to be fertile.

We observed subtle phenotypic differences between *Mlh1*$^{-/-}$ and *Mlh3*$^{-/-}$ mice. In *Mlh1*$^{-/-}$ mice, meiotic disruption occurs abruptly, with complete spermatocyte loss at diplonema, whereas in *Mlh3*$^{-/-}$ mice, the apoptotic switch is less stringent and sizable numbers of spermatocytes progress further into metaphase I. Preloading of Mlh3 is required for binding of Mlh1 to pachytene chromosomes, and loss of Mlh3 causes complete failure or loss of recombination nodules at mid pachynema. Together these observations suggest that maintenance of chiasmata requires Mlh1–Mlh3 heterodimers through one of two possible mechanisms. Either loss of Mlh3 alone causes loss of chiasmata and the associated proteins (including Mlh1), or loss

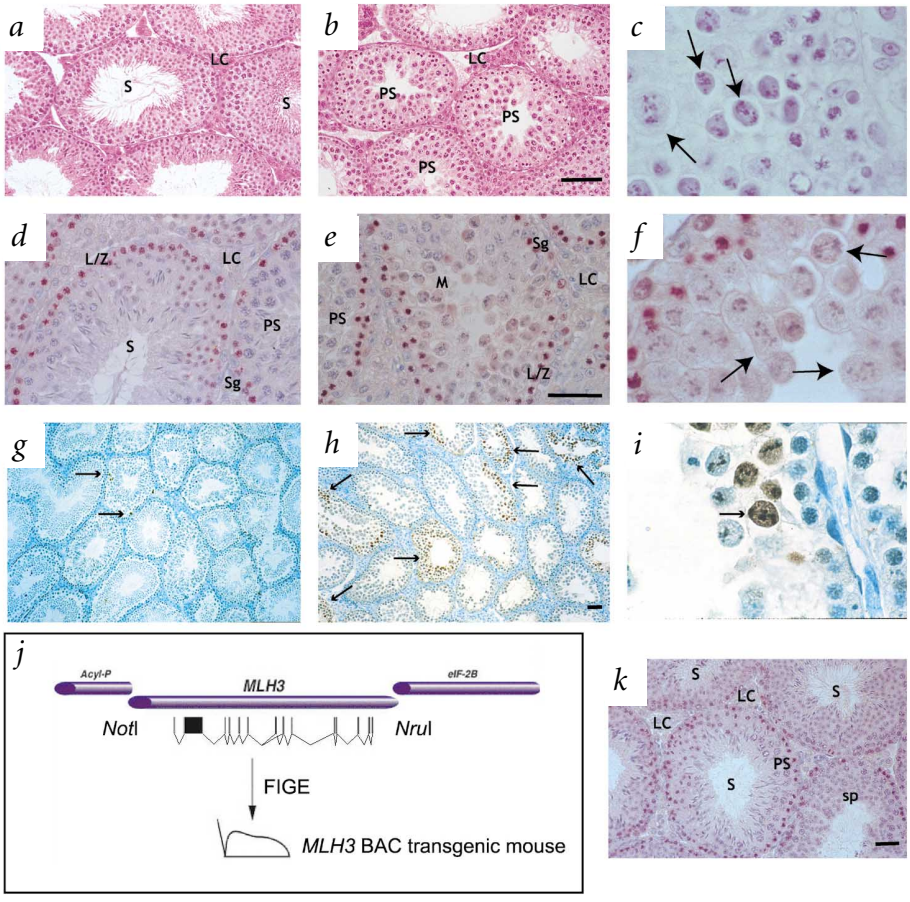

Fig. 3 Testicular histology of wildtype (left panels) and *Mlh3*$^{-/-}$ male mice (middle and right panels). ***a–c***, Staining of testis sections with hematoxylin and eosin shows absence of spermatozoa and an accumulation of pachytene spermatocytes and abnormal metaphase cells (arrows) in *Mlh3*$^{-/-}$ males (*b*,*c*), as compared with normal seminiferous epithelium observed in testes from wildtype males (*a*). ***d–f***, Localization of Gcna1 (pink precipitate) in the seminiferous tubule of wildtype (*d*) and *Mlh3*$^{-/-}$ (*e*,*f*) males shows failure of spermatogenesis at pachynema and the accumulation of abnormal metaphase I cells (*f*; arrows). ***g–i***, The failure of spermatogenesis in *Mlh3*$^{-/-}$ males is accompanied by an increase in apoptosis, as indicated by increased TUNEL staining (brown precipitate; small arrows) in the *Mlh3*$^{-/-}$ testis (*h*,*i*) as compared with wildtype (*g*) controls. ***j***, Strategy for generating *MLH3* genomic transgenic mice (*MLH3 Tg*$^{+}$) to rescue *Mlh3*$^{-/-}$ phenotypes. FIGE, field-inversion gel electrophoresis. ***k***, Spermatogenesis in *Mlh3*$^{-/-}$*MLH3 Tg*$^{+}$ mice proceeds normally, as indicated by the spermatozoa (S) in the seminiferous tubular lumen. Northern analysis using sequences specific for the 3′ UTR of *MLH3* confirmed the generation of three independent lines of transgenic mice expressing an intact *MLH3* mRNA transcript, and immunoblotting confirmed expression of the full-length MLH3 protein. Each of these three lines expressed *MLH3* mRNA at 1.0–1.5 times the endogenous level in wildtype mice (data not shown). LC, Leydig cells; L/Z, leptotene/zygotene spermatocytes; M, metaphase I spermatocyte; PS, pachytene spermatocyte; S, spermatozoa; Sg, spermatogonia; Sp, spermatids. Scale bars, 100 μm.

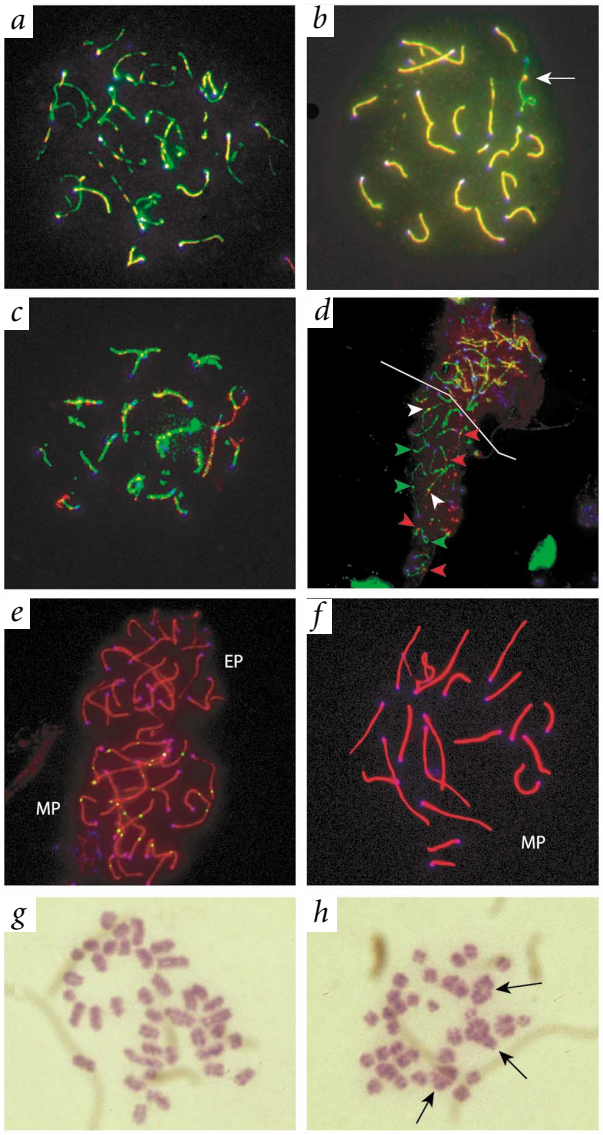

Fig. 4 Normal chromosomal synapsis in spermatocytes from adult *Mlh3*$^{-/-}$ male mice is followed by failure to maintain homologous pairing at metaphase. ***a***,***b***, Chromosomal synapsis in spermatocytes from *Mlh3*$^{-/-}$ males is monitored by the colocalization of Cor1 (FITC, green), which localizes to axial elements along each homolog, and Syn1 (TRITC, red), which is an integral component of the central element of the synaptonemal complex that tethers the two homologs together. Syn1 associates with homologous chromosome cores at zygonema (*a*), and the synaptonemal complex becomes fully formed at pachynema (*b*) when all chromosomes are fully synapsed (yellow). Only the XY bivalent remains unsynapsed, except at the pseudoautosomal (PA) region (arrow). ***c***, Correct synapsis in *Mlh3*$^{-/-}$ males is also indicated by the localization of Rad51 (TRITC, red) on unsynapsed portions of the synaptonemal complex (FITC, green) and by the loss of Rad51 in synapsed portions of the chromosomes in early pachynema. ***d***, In wild-type spermatocyte preparations, Rpa (TRITC, red) localizes to synaptonemal complexes (FITC, green) during early pachynema (upper cell) before Mlh3 foci become evident. As pachynema progresses, Rpa foci are lost gradually and Mlh3 foci (FITC, green) become apparent. A few Mlh3–Rpa double foci (white arrowheads) are easily distinguishable from single Mlh3 (green arrowheads) or single Rpa (red arrowheads) foci. ***e***,***f***, Localization of Mlh1 using mouse monoclonal antibody against Mlh1 (FITC, green) on meiotic chromosomes labeled with polyclonal rabbit antisera raised against Cor1 and Syn1 (TRITC, red). *e*, Mlh1 localizes to meiotic chromosomes from wildtype spermatocytes during mid pachynema, as reported[12,19]. By contrast, no Mlh1 foci are found on spermatocytes from *Mlh3*$^{-/-}$ males (*f*, $n = 3$ mice), despite the frequent appearance of mid pachytene spermatocytes. EP, early pachynema; MP, mid pachynema. In *a–f*, the centromeres (which are telomeric in mice) are labeled in blue with autoimmune serum against CREST (Cy5). ***g***,***h***, Two Giemsa-stained, air-dried chromosome preparations of metaphase I spermatocytes from *Mlh3*$^{-/-}$ males, showing failure to maintain crossovers in all but a few cases (arrows in *h*). Note the appearance of more than 20 chromosome structures, which indicates premature desynapsis in these cells.

of the Mlh1–Mlh3 heterodimer causes destabilization of chiasmata and loss of recombination nodules. Reports of 90% reductions in *Mlh1*$^{-/-}$ crossovers at metaphase[12,19] support the requirement for Mlh1 in maintaining chiasmata, but the absence of recombination nodules at pachynema in *Mlh3*$^{-/-}$ mice seems to suggest that Mlh3 is of primary importance and recruits Mlh1 as part of a MutL complex. These phenotypic differences suggest that different 'checkpoints' exist for Mlh1 and Mlh3. One explanation is that absence of both Mlh1 and Mlh3 reduces the number of crossovers, which, in turn, reduces the efficiency of the checkpoint that exists at diplonema. But absence of Mlh1 does not by itself totally compromise crossover frequency, and therefore the stringency of the checkpoint is maintained. In the absence of both Mlh1 and Mlh3 in *Mlh3*$^{-/-}$ animals, the meiotic disruption is similar, but the compounded failure of checkpoint activation results in a more progressive loss of spermatocytes throughout meiosis I and beyond. Alternatively, Mlh1 and Mlh3 might also trigger checkpoints directly so that loss of both would reduce the apoptosis. These models are consistent with the lower number of crossovers observed in *Mlh1*$^{-/-}$ mice as compared to wild type[12,19] and with the hypothesis that Mlh1 acts as a meiotic checkpoint regulator[20].

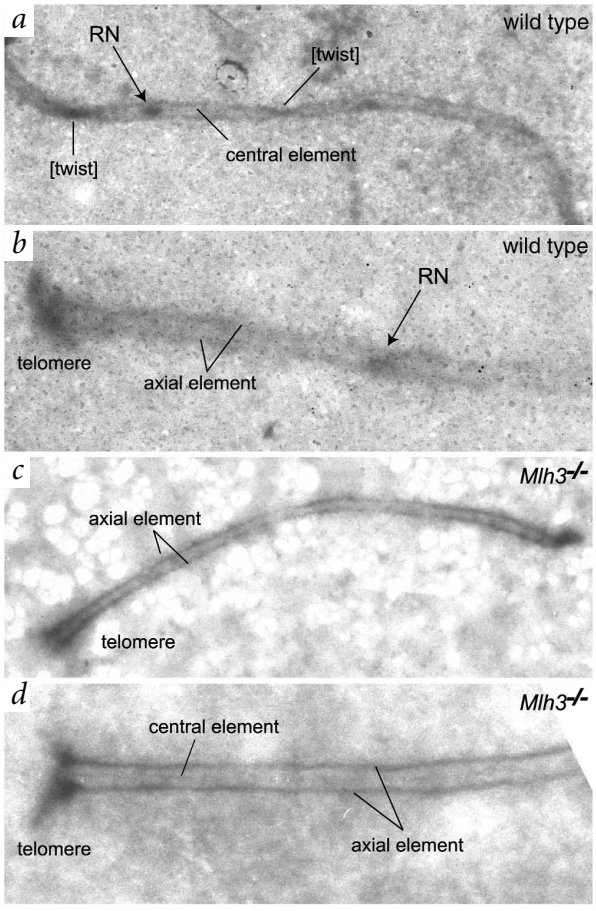

Fig. 5 Electron micrographs of surface-spread chromosomes. Shown are pachytene chromosomes from wildtype (***a***,***b***) and *Mlh3*$^{-/-}$ (***c***,***d***) stained with PTA (which stains some protein components of the chromosome cores, the central elements and the recombination nodules, RN), demonstrating fully synapsed bivalent chromosomes. In the wild type, electron-dense recombination nodules are easily visible between the two axial elements of the synaptonemal complex. Typically one or two recombination nodules are visible on each chromosome, depending on the length, and are readily differentiated from the chromosome twists that occur during the spreading procedure. By contrast, recombination nodules are not observed on pachytene spreads from *Mlh3*$^{-/-}$ males (at least 50 nuclei were examined from two mice).

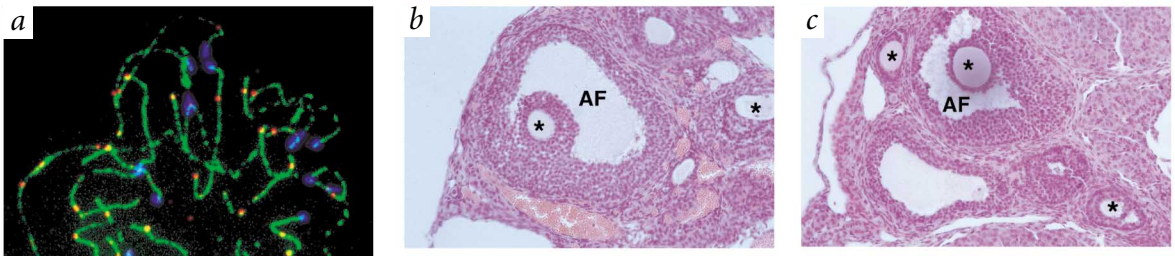

Fig. 6 Normal ovarian morphology in *Mlh3*$^{-/-}$ female mice and localization of Mlh3 on chromosomes from ovaries of embryonic day 19 females. ***a***, Localization of Mlh3 on meiotic chromosomes from pachytene oocytes taken from E19 female embryos and stained with antibodies against Cor1 (TRITC, red), Mlh3 (FITC, green) and CREST (Cy5, blue), as described in Fig. 4. Mlh3 foci are present on pachytene oocyte chromosomes at a frequency similar to that seen on spermatocyte spread chromosomes (average 1–3 foci per pachytene chromosome). ***b***,***c***, Sections of ovary from wildtype (*b*) and *Mlh3*$^{-/-}$ (*c*) adult female mice stained with hematoxylin and eosin, showing normal follicular development in the absence of Mlh3. AF, antral follicle; *, oocyte.

In this model, Pms2 might be required to load the Mlh1–Mlh3 heterodimer onto chromosomes; thus, Pms2 would load first, presumably at Msh4–Msh5 foci in zygonema. The gradual loss of Msh4–Msh5 foci as synapsis proceeds might reflect a replacement of Pms2 by Mlh1–Mlh3 at some foci. An absence of Pms2 might result in an alteration in the number of Mlh1–Mlh3 foci, thereby resulting in checkpoint activation. In this model, the preloaded Pms2 could be functionally active, which is consistent with reports that monomeric Pms2, unlike monomeric MutL, can bind DNA and can effect hydrolysis of ATP[21]. If our model is correct, then Mlh1–Pms2 or Mlh1–Pms1 complexes may substitute partially for Mlh1–Mlh3 complexes during diplonema, but in a manner that is insufficient for successful completion of meiosis and escape from an apoptotic fate. Future experiments with mice deficient in more than one mismatch-repair gene will be required to resolve this question.

Methods

Generation of Mlh3 antisera. We coupled peptides comprising the 20 carboxyl-terminal amino acids of Mlh3 to keyhole limpet hemocyanin carrier (Zymed) and injected them into NZW female rabbits. Polyclonal antisera were affinity purified using the same Mlh3 peptide that was used to prime the rabbit immune response coupled to Sepharose.

Methods for Mlh3 BAC isolation and sequencing. Two C57BL/6J mouse RPCI-23 BAC libraries, RPCI-23 207k15 and RPCI-23 9b17 (ref. 22) were screened using 'overgo' probes specific for *Mlh3*. We isolated positive clones, subjected them to fingerprint analysis on the basis of restriction enzyme digests, and selected overlapping clones for sequencing the whole *Mlh3* genomic region[23]. The selected BAC clones were sequenced by shotgun using described techniques[24–26]. We edited and assembled sequences with the Phred/Phrap/Consed suite of programs[27].

Generation of an Mlh3-null allele in embryonic stem cells. A genomic fragment of 3.6 kb containing exon 1, exon 2 and the 5′ flanking sequence of *Mlh3* derived from a 129 Sv/Ev phage library was subcloned into the *Not*I site of pNT *loxP*, and a genomic fragment of 6.3 kb of the *Mlh3* intron was subcloned into the *Eco*RI site. This construct places the PGK promoter–neomycin cassette, flanked on both 5′ and 3′ ends by *loxP* sites, in the same transcriptional orientation as *Mlh3*. The targeting vector (50 μg) was linearized at the single *Not*I side and electroporated into 2.0×10^7 129 Sv/Ev embryonic stem (ES) cells. The ES cells were selected in neomycin, and resistant colonies were isolated after 10 d of selection. We screened genomic DNA from individual colonies by Southern analysis using genomic DNA digested with *Eco*RI and a 5′ flanking probe. Homologous recombinant ES cell clones testing positive in this screen were confirmed by Southern analysis using a probe external to the targeting vector from *Mlh3* intron 3. Sequences are available from the authors on request.

Mice were handled according to institutional guidelines for the humane care and use of experimental animals, and with approval for all studies from the appropriate Institutional Animal Care Committees at the Albert Einstein College of Medicine and the National Human Genome Research Institute. Mice were fed *ad libitum* with standard pet chow and water, and housed under conditions of controlled light (12 h/12 h light/dark cycle) and temperature (27 °C).

Northern-blot analysis. For analysis of *Mlh3* expression, testis RNA was obtained from mice *Mlh3*$^{-/-}$, *Mlh3*$^{+/-}$ and wildtype mice. Poly(A) RNA was separated on 1.0% agarose formaldehyde gels and transferred to a nylon membrane. A full-length *Mlh3* cDNA probe was labeled and hybridized to determine mRNA expression. We assessed mRNA quality and quantity by means of a β-actin probe.

Microsatellite instability analysis. DNA was extracted from Mlh3$^{-/-}$ embryonic fibroblast cultures and analyzed for microsatellite instabili-

Table 1 • Development of oocytes from wildtype and *Mlh*$^{-/-}$ females after fertilization *in vitro* with wildtype spermatozoa[a]

Hours after insemination	Appearance	wildtype	Mlh3$^{-/-}$
0	number of oocytes retrieved	65	43
	normal	93.8 (61)[b]	88.4 (38)
4	first polar body	92.3 (60)	55.8 (24)
	abnormal	1.5 (1)	32.6 (14)
8	first polar body only	64.6 (42)	25.6 (11)
	second polar body	24.1 (15)	18.6 (8)
	abnormal	4.6 (3)	11.6 (5)
22	first polar body only	4.6 (3)	20.9 (9)
	second polar body	72.3 (47)	18.6 (8)
	two-cell embryos	10.8 (7)	0 (0)
	abnormal	0 (0)	4.6 (2)
34	first polar body only	0 (0)	16.3 (7)
	second polar body	19.3 (11)	13.9 (6)
	two-cell embryos	50.8 (33)	7.0 (3)
	four-cell embryos	15.4 (10)	0 (0)
	abnormal	4.6 (3)	2.3 (1)

[a]Oocytes were retrieved from 4-week female mice and subjected to *in vitro* fertilization with wildtype sperm that had been allowed to capacitate for 2 h before insemination. [b]Results are reported as percentages, with actual numbers given in parentheses.

ty using markers *D1Mit36*, *D7Mit91*, *D14Mit15*, JH102, JH103 and JH104 as described[15,28]. In addition, three other tetranucleotide markers (sequences available on request) were also tested using the same conditions. Amplified PCR products were separated on an ABI 377 instrument, and their instability was recorded as the percentage of reactions that yielded an abnormal size product. Genomic DNA from *Ccs*I normal tissue and tumors, which show satellite instability[15], was used as a positive control. The size shift in one allele was observed using the AAAG-I marker.

Histology. Ovaries and testes from adult mice were fixed in Bouin's fixative or 4% buffered formalin for 1–12 h, depending on the size of specimen. We processed fixed tissues for immunohistochemistry by routine methods and sectioned the paraffin-embedded tissues at 5 μm.

Chromosome analysis. For analysis of prophase I chromosome configurations and protein localization, we prepared spermatocyte and oocyte spreads as described[8,10]. For analysis of male meiosis, we removed testes from adult wildtype and *Mlh3*$^{-/-}$ males. For analysis of female meiosis, embryonic ovaries were removed between E16 and E19.

For electron micrographic analysis of chromosomes from mouse, we spread spermatocytes onto plastic-coated slides. After being fixed in 2% paraformaldehyde, chromosomes were washed in 0.4% Photoflo (Kodak) and then dried in air. Chromosomes were treated with DNase (1 μg/ml in DMEM medium), washed and dried before being applied to electron microscopy grids (by floating the plastic sheets off the microscope slides onto the surface of ultrapure water, and then picking up the sheets onto nickel electron microscopy grids). The grids were stained with 4% phosphotungstic acid (PTA; 1:3 in 95% ethanol) for 10–20 min and washed in 95% ethanol.

Immunofluorescence and immunohistochemistry. Slides containing chromosome spreads were subjected to immunofluorescence staining as described[8,10]. We used the following primary antibodies: a mouse monoclonal antibody against Cor1, a component of the mouse synaptonemal complex (1:1,000); a mouse monoclonal antibody raised against human Rpa that crossreacts with the mouse protein (1:400); a rabbit polyclonal antibody raised against mouse Rad51 (1:500); and a mouse monoclonal antibody against human Mlh1 (1:50). For immunohistochemistry, paraffin sections were incubated with a rat hybridoma supernatant against germ cell nuclear antigen-1 (Gcna-1)[29] or stained with hematoxylin and eosin to reveal more detailed histological architecture. Secondary antibodies for immunofluorescence were conjugated to fluorescein isothiocyanate (FITC), tetramethylrhodamine isothiocyanate (TRITC) or cyanine-5 (Cy5), all from Jackson ImmunoResearch. Control labeling of the centromeres was performed using human autoimmune serum from individuals with scleroderma associated with calcinosis, Raynaud phenomenon, esophageal dysmotility, sclerodactyly and telangiectasia (CREST) syndrome. Where two antibody conjugates with the same fluorochrome were used, one primary antibody (usually the antibody against Cor1) was at approximately one tenth the normal concentration and the other was at its regular concentration. Apoptosis assays were performed using an ApopTag TUNEL (terminal deoxynucleotidyltransferase biotin–dUTP nick end-labeling) kit from Intergen.

GenBank accession numbers. Mouse RPCI-23 BAC libraries: RPCI-23 207k15 (4.1× coverage), AC079735; RPCI-23 9b17 (5.9× coverage), AC068067.

Note: Supplementary information is available on the Nature Genetics website.

Acknowledgments

We thank G. Elliott and A. Becker for help with mouse studies; M. Liskay and W. Edelmann for critically reading this manuscript; G. Enders for antibodies; and N. Kolas for discussions and advice. This work was supported by the Albert Einstein College of Medicine (P.E.C.), National Human Genome Research Institute intramural funds and New Faculty start-up funds through the University of California, Irvine (S.M.L.).

Competing interests statement

The authors declare that they have no competing financial interests.

Received 11 March; accepted 16 May 2002.

1. Modrich, P. & Lahue, R. Mismatch repair in replication fidelity, genetic recombination, and cancer biology. *Annu. Rev. Biochem.* **65**, 101–133 (1996).
2. Kolodner, R.D. & Marsischky, G.T. Eukaryotic DNA mismatch repair. *Curr. Opin. Genet. Dev.* **9**, 89–96 (1999).
3. Wang, T.F., Kleckner, N. & Hunter, N. Functional specificity of MutL homologs in yeast: evidence for three Mlh1-based heterocomplexes with distinct roles during meiosis in recombination and mismatch correction. *Proc. Natl Acad. Sci. USA* **96**, 13914–13919 (1999).
4. Hollingsworth, N.M., Ponte, L. & Halsey, C. MSH5, a novel MutS homolog, facilitates meiotic reciprocal recombination between homologs in *Saccharomyces cerevisiae* but not mismatch repair. *Genes Dev.* **9**, 1728–1739 (1995).
5. Ross-Macdonald, P. & Roeder, G.S. Mutation of a meiosis-specific MutS homolog decreases crossing over but not mismatch correction. *Cell* **79**, 1069–1080 (1994).
6. Her, C., Wu, X., Wan, W. & Doggett, N.A. Identification and characterization of the mouse MutS homolog 5: *Msh5*. *Mamm. Genome* **10**, 1054–1061 (1999).
7. de Vries, S.S. *et al*. Mouse MutS-like protein Msh5 is required for proper chromosome synapsis in male and female meiosis. *Genes Dev.* **13**, 523–531 (1999).
8. Kneitz, B. *et al*. MutS homolog 4 localization to meiotic chromosomes is required for chromosome pairing during meiosis in male and female mice. *Genes Dev.* **14**, 1085–1097 (2000).
9. Paquis-Flucklinger, V. *et al*. Cloning and expression analysis of a meiosis-specific MutS homolog: the human MSH4 gene. *Genomics* **44**, 188–194 (1997).
10. Edelmann, W. *et al*. Mammalian MutS homologue 5 is required for chromosome pairing in meiosis. *Nature Genet.* **21**, 123–127 (1999).
11. Hunter, N. & Borts, R.H. Mlh1 is unique among mismatch repair proteins in its ability to promote crossing-over during meiosis. *Genes Dev.* **11**, 1573–1582 (1997).
12. Baker, S.M. *et al*. Involvement of mouse Mlh1 in DNA mismatch repair and meiotic crossing over. *Nature Genet.* **13**, 336–342 (1996).
13. Baker, S.M. *et al*. Male mice defective in the DNA mismatch repair gene *PMS2* exhibit abnormal chromosome synapsis in meiosis. *Cell* **82**, 309–319 (1995).
14. Edelmann, W. *et al*. Meiotic pachytene arrest in MLH-1-deficient mice. *Cell* **85**, 1125–1134 (1996).
15. Lipkin, S.M. *et al*. MLH3: a DNA mismatch repair gene associated with mammalian microsatellite instability. *Nature Genet.* **24**, 27–35 (2000).
16. Moens, P.B. *et al*. The time course and localization of recombination-related proteins at meiosis in the mouse conform to models that can resolve the early DNA-DNA interactions without reciprocal recombination. *J. Cell Sci.* **115**, 1611–1622 (2002).
17. Anderson, L.K., Reeves, A., Webb, L.M. & Ashley, T. Distribution of crossing over on mouse synaptonemal complexes using immunofluorescent localization of MLH1 protein. *Genetics* **151**, 1569–1579 (1999).
18. Flores-Rozas, H. & Kolodner, R.D. The *Saccharomyces cerevisiae* MLH3 gene functions in MSH3-dependent suppression of frameshift mutations. *Proc. Natl Acad. Sci. USA* **95**, 12404–12409 (1998).
19. Woods, L.M. *et al*. Chromosomal influence on meiotic spindle assembly: abnormal meiosis I in female Mlh1 mutant mice. *J. Cell Biol.* **145**, 1395–1406 (1999).
20. Cohen, P.E. & Pollard, J.W. Regulation of meiotic recombination and prophase I progression in mammals. *BioEssays* **23**, 996–1009 (2001).
21. Guarne, A., Junop, M.S. & Yang, W. Structure and function of the N-terminal 40 kDa fragment of human PMS2: a monomeric GHL ATPase. *EMBO J.* **20**, 5521–5531 (2001).
22. Osoegawa, K. *et al*. Bacterial artificial chromosome libraries for mouse sequencing and functional analysis. *Genome Res.* **10**, 116–128 (2000).
23. Marra, G. *et al*. Mismatch repair deficiency associated with overexpression of the MSH3 gene. *Proc. Natl Acad. Sci. USA* **95**, 8568–8573 (1998).
24. Green, E.D. Strategies for the systematic sequencing of complex genomes. *Nature Rev. Genet.* **2**, 573–583 (2001).
25. Ellsworth, R.E. *et al*. Comparative genomic sequence analysis of the human and mouse cystic fibrosis transmembrane conductance regulator genes. *Proc. Natl Acad. Sci. USA* **97**, 1172–1177 (2000).
26. Touchman, J.W. *et al*. The genomic region encompassing the nephropathic cystinosis gene (CTNS): complete sequencing of a 200-kb segment and discovery of a novel gene within the common cystinosis-causing deletion. *Genome Res.* **10**, 165–173 (2000).
27. Ewing, B., Hillier, L., Wendl, M.C. & Green, P. Base-calling of automated sequencer traces using phred. I. Accuracy assessment. *Genome Res.* **8**, 175–185 (1998).
28. Edelmann, W. *et al*. The DNA mismatch repair genes Msh3 and Msh6 cooperate in intestinal tumor suppression. *Cancer Res.* **60**, 803–807 (2000).
29. Wang, D. & Enders, G.C. Expression of a specific mouse germ cell nuclear antigen (GCNA1) by early embryonic testicular teratoma cells in 129/Sv-Sl/+ mice. *Cancer Lett.* **100**, 31–36 (1996).